Scilight

*Smart Energy Systems*

https://www.sciltp.com/journals/ses

*Article*

# Design and Performance Analysis of a Type-2 FLC Controller for a Fuel Cell Electric Vehicle Powertrain

Meltem Fistikçioğlu [1,2], Doğukan Mehmet Kilinç [1,3] and Gökay Bayrak [4,*]

[1] Electrical and Electronics Engineering, Graduate School, Bursa Technical University, Bursa 16300, Türkiye
[2] System Modeling and Control Engineer, FIGES Inc., Bursa 16300, Türkiye
[3] AI and Machine Learning Engineer, FIGES Inc., Bursa 16300, Türkiye
[4] Department of Electrical and Electronics Engineering, Electric Vehicles Application and Research Center, Bursa Technical University, Bursa 16300, Türkiye
* Correspondence: gokay.bayrak@btu.edu.tr

**How To Cite:** Fistikçioğlu, M.; Kilinç, D.M.; Bayrak, G. Design and Performance Analysis of a Type-2 FLC Controller for a Fuel Cell Electric Vehicle Powertrain. *Smart Energy Systems* **2026**, *1*(1), 3

Received: 1 February 2026
Revised: 2 April 2026
Accepted: 9 April 2026
Published: 20 April 2026

**Abstract:** The energy industry has been forced to target zero carbon emissions due to increasing global energy demand and environmental problems caused by the depletion of fossil fuel resources. Proton Exchange Membrane Fuel Cells (PEMFC) are one of the clean energy and strategic options for the future because of their low operating temperature, flexible design, and high energy density. However, because of activation, ohmic, and concentration losses resulting from the electrochemical reactions in its stacks, PEMFC displays a non-linear output characteristic. Moreover, due to its sensitivity to load changes, it becomes even more difficult to achieve reliable voltage regulation that meets industry standards. In this study, the performance of two different control architectures (Classic Proportional-Integral (PI) and Type-2 Fuzzy Logic (T2FLC)) developed to regulate the output voltage of a PEMFC stack operating under dynamic load conditions to a 96-volt reference value via a DC-DC Boost Converter using MATLAB/Simulink is compared. In contrast to previous research, this paper proposes a Gain Scheduling approach to improve the transient reaction speed of intelligent controllers while removing the oscillation problem that occurs in the steady-state area and reduces power quality. This method dynamically optimizes the controller gains while continuously monitoring the amount of the error signal in the produced system. The simulation findings show that although Type-2 Fuzzy Controllers with Footprint of Uncertainty (FOU) structure performed better against noise, the fixed gain PI controller failed at different operating points**.** In both scenarios, the Gain Scheduling Type-2 Fuzzy Logic structure produced a power flow that minimized steady-state oscillation and mitigated instantaneous power stress, thereby reducing factors that contribute to thermal degradation, by capturing the 96-volt reference value in around 0.3 s. It was successful in controlling the 96-volt target with an average steady-state error of 0.30% during the 0–1 s simulation period and 0.04% during the 0.3–1 s simulation period

**Keywords:** fuel cell electric vehicle; PEM fuel cell; DC-DC boost converter; Type-2 fuzzy logic; gain scheduling

## 1. Introduction

Fuel cells are currently assuming a pivotal role within the energy industry as a potential successor to fossil fuel-based generators for clean energy production. Distinct from renewable technologies such as wind and solar power, they are capable of delivering optimal service without geographical constraints. This capability ensures

that energy generation remains independent of geographical conditions, weather patterns, specific locations, or environmental factors. Within the array of fuel cell technologies, Proton Exchange Membrane Fuel Cells (PEMFCs) stand out as the most prominent option, primarily due to their high-power densities and low operating temperatures. Nevertheless, the effective utilization of this system mandates the rigorous selection of accurate models and the most suitable supporting technologies.

Aimani developed a model to analyze the parameters affecting the efficiency of PEMFC systems in the MATLAB/Simulink environment and validated the theoretical models with the obtained polarization curves [1]. On the technological comparison side, Fandi et al. compared the simulation results of vehicles with different fuel types specifically for postal delivery vehicles. In this specific scenario, they compared Hydrogen Fuel Cell Electric Vehicles (HFCEVs) with Battery Electric Vehicles (BEVs) under standard driving cycles, highlighting the efficiency advantages of battery systems and examining the range and refueling time potential of fuel cell systems [2].

Nonlinear power outputs, which develop depending on environmental conditions, are the biggest challenge encountered in the characteristics of PEMFC and photovoltaic (PV) systems. In this case, Maximum Power Point Tracking (MPPT) algorithms play an important role in ensuring that the system uses its maximum power at any given moment. In their study classifying existing MPPT methods for microgrid applications, Ko et al. emphasized that while traditional methods such as Constant Voltage (CV) and Switch & Observe (P&O) are simple, artificial intelligence-based methods are superior in dynamic conditions [3]. Indeed, current issues in the literature focus on solving the trade-off problems between tracking speed and stability of traditional methods. As a reference, Derbeli et al. provided an effective solution to this problem with their fuzzy logic controller implemented on the dSPACE platform; they radically improved the system's performance by reducing steady-state oscillations by 73.2%, response time by 81.5%, and overshoot by 52.9% compared to the commonly used Incremental Conductivity (IncCond) algorithm. Similarly, Harrag and Messalti developed a variable step size and "Neuro-Fuzzy" based MPPT approach to increase the system response speed and minimize power losses [4,5]. Managing uncertainties in controller design is also a critical research topic. Doğan et al. proposed a Type-3 Fuzzy Logic (FLT3) structure to manage uncertainties in parameters such as temperature and gas pressure changes, and it was proven that this structure provides a much faster settling time (0.05) compared to Type-2 and P&O controllers [6]. Along with these studies, Rezk and Fathy achieved high tracking efficiency results under different load conditions with the variable step size incremental resistor (VSS-INR) technique [7], and Derbeli et al. achieved similar results with Reference Current Estimator based approaches [8]. In terms of microgrid integration, Kim et al. optimized the system according to working regions based on fuzzy logic rules [9], while Luta and Raji showed that the highest power was achieved with 99.39% efficiency with Particle Swarm Optimization (PSO) in their analyses on a 53-kW stack, but Mamdani type fuzzy controller offered more stable dynamic responses [10].

In addition to the generated power, advanced power electronics and inner-loop control strategies are required for the regulation of this power and the protection of system components. Charaabi et al. proposed a two-stage Sliding Mode Control (SMC) structure to control DC-DC boost converters in PV systems and minimized output voltage ripples with a high efficiency of 99.87% [11]. At this stage, precision in the control of reactant gases is also of vital importance to extend the lifespan of the fuel cell stack. In this regard, Benchouia et al. accelerated the transient response of the system by overcoming the slow performance of PID controllers with an adaptive fuzzy logic controller (AFLC) that optimizes gas flow rates [12]. To prevent membrane damage, which is an even more critical safety issue, Abbaspour et al. developed a robust adaptive neural network controller that balances oxygen and hydrogen partial pressures; with this method, they increased the reliability of the system by reducing the pressure control error from levels of 16% to 6% [13]. As for specific fields requiring high reliability such as aviation, Gwon et al. conducted a study. With the Double-Input Single-Output (DISO) converter topology they developed for Lift-Cruise UAVs, they presented a fault-tolerant structure capable of transferring the load to the other within 0.9 ms when one stack fails [14].

Finally, there are hybrid systems in which fuel cells are utilized in conjunction with other energy sources such as batteries and supercapacitors. Energy Management Systems (EMS), which manage the energy flow in these systems, are the determinants of overall efficiency. Here, hybrid and optimization-based strategies come to the forefront. Du et al. developed a strategy that reduces hydrogen consumption by 14.98% and the computational burden by 96% by combining a real-time applicable ANFIS structure with a Dynamic Programming (DP) structure that provides global optimization [15]. It has been observed in the literature review that meta-heuristic algorithms are also frequently used for the optimization of EMS parameters. Mazouzi et al. optimized the membership functions created in fuzzy logic using Genetic Algorithms (GA) and achieved a 28.5% improvement in fuel usage [16]. Similarly, Luo and Chung proposed a fuzzy EMS reinforced with the "Dung Beetle Optimizer" (DBO) algorithm for electric vehicles, thereby maintaining the battery State of Charge (SOC) more effectively under dynamic acceleration conditions [17]. To manage unplanned uncertainties that may be encountered in the future, Yuan et al.

presented a Reinforcement Learning-based dual Model Predictive Control (MPC) structure and succeeded in keeping fuel cell efficiency above 45% [18]. In grid-connected systems, Garcia et al. and Çakmak et al. improved grid power quality (THD) using ANFIS and fuzzy logic-based approaches, respectively, and achieved economic optimization by considering dynamic pricing and generation forecasts [19,20]. Additionally, Bizon and Thounthong achieved gains of up to 12% in fuel economy thanks to a load tracking strategy combined with extremum seeking control [21]. Furthermore, FCEV powertrain applications incorporating intelligent controllers are becoming increasingly popular in the literature [22,23].

On the other hand, when examining control strategies in the literature, the fundamental distinction between Type-1 and Type-2 fuzzy logic systems relies on their uncertainty management capacity. In conventional Type-1 Fuzzy Logic systems, membership degrees are expressed as crisp values between 0 and 1. Although this structure is successful in general control tasks, it is not sufficiently effective in systems where high noise and variable parameters exist. In contrast, Type-2 Fuzzy Logic systems model the membership degree itself within a fuzzy range thanks to the "footprint of uncertainty" in their membership functions. Thus, they can cope with nonlinearities and external disturbances in the system in a more robust manner compared to the Type-1 Fuzzy Logic method [6]. However, this high uncertainty tolerance offered by Type-2 systems brings along significant computational burden and design complexity. Therefore, Type-1 systems are preferred to reduce complexity and lower processor costs. The performance gaps are attempted to be bridged by performing parameter optimization with meta-heuristic algorithms such as Genetic Algorithm or Dung Beetle Optimizer [16,17].

While these previous studies extensively cover system-level optimization and tuning strategies, the inner-loop voltage regulation of the DC-DC boost converter remains a critical challenge for PEMFC powertrains. Fuel cells exhibit highly nonlinear polarization characteristics and slow thermodynamic responses. Under the dynamic load variations typical of electric vehicles, classical fixed-gain controllers, such as the industry-standard Proportional-Integral (PI) controller, fail to accommodate these wide operating ranges, leading to degraded power quality and increased thermal stress. On the other hand, intelligent controllers like Type-1 Fuzzy Logic are limited in modeling high levels of system uncertainty. Therefore, achieving a robust, fast, and oscillation-free voltage regulation for PEMFCs under severe dynamic conditions remains a specific research gap that necessitates a more adaptive control architecture.

To address this specific gap, this paper proposes a novel Gain-Scheduled Interval Type-2 Fuzzy Logic Controller (GS-IT2-FLC) for the voltage regulation of a PEMFC-based FCEV powertrain. The explicit contributions of this study are outlined as follows:

1. Application of Interval Type-2 Fuzzy Logic for PEMFC Voltage Regulation: An IT2-FLC is designed to inherently capture and manage the highly nonlinear characteristics and parameter uncertainties of the PEMFC, utilizing its Footprint of Uncertainty (FOU) to outperform standard PI and Type-1 Fuzzy controllers.
2. Error-Driven Hysteresis Adaptive Gain Scheduling (AGS): A novel dual-threshold hysteresis gain scheduling mechanism is introduced. It dynamically optimizes the controller gains based on the error magnitude, allowing the system to react aggressively to abrupt load changes while effectively suppressing steady-state oscillations.
3. Comprehensive Hardware-Aware Performance Analysis: The proposed architecture is quantitatively compared against the industry-standard PI controller under severe dynamic load conditions. The evaluation explicitly highlights the engineering implications, demonstrating a significant reduction in voltage overshoot (by approximately 68.4%) and power stress, thereby enhancing the long-term reliability and operational lifespan of the fuel cell stack.

## 2. System Modelling

In the proposed system architecture, a Proton Exchange Membrane Fuel Cell (PEMFC) is utilized as the primary clean energy source. Within this configuration, the output of the fuel cell interfaces with distinct control units; consequently, the control mechanism depicted in Figure 1 has been established to regulate the system and step up the voltage to the targeted level via a DC-DC Boost Converter.

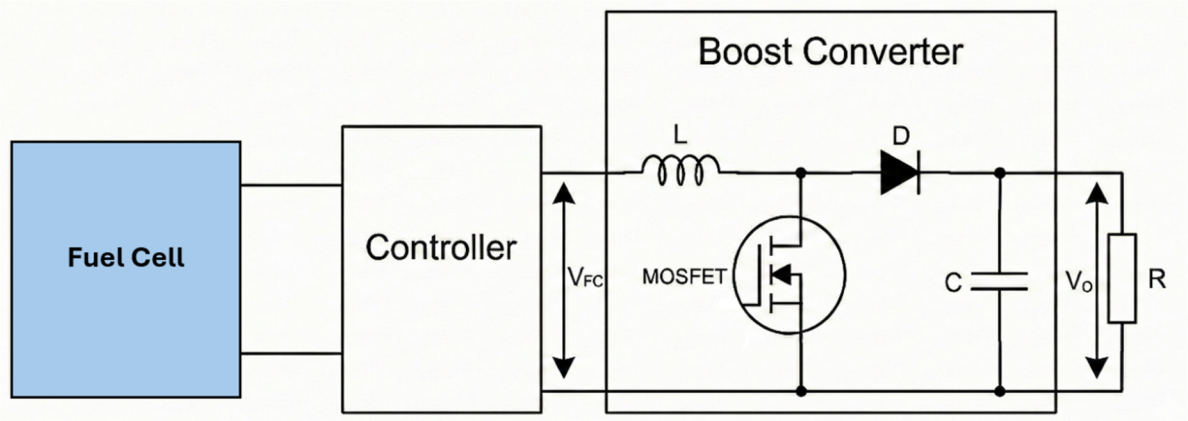


**Figure 1.** System design.

### *2.1. PEMFC Characteristics*

PEM fuel cells are defined as electrochemical devices capable of directly converting chemical energy into electrical energy. In this study, a fuel cell model was developed within the MATLAB/Simulink environment. The implemented model represents a modified version of the approach recommended by [10], wherein reactive flow dynamics are considered negligible.

The voltage resulting from these electrochemical reactions is expressed by the Nernst equation, as shown in Equation (1) [10]:

$$E_n = 1.229 + (T - 298) \times \frac{-44.43}{2 \times F} + \frac{R \times T}{2 \times F} \times \ln\left(P_{H_2} \times P_{O_2}^{\frac{1}{2}}\right) \quad (1)$$

where $P_{H_2}$ and $P_{O_2}$ enote the partial pressures of hydrogen and oxygen, respectively. Furthermore, $T$, $F$ and $R$ represent the temperature, the Faraday constant, and the ideal gas constant. These partial pressures are defined as functions of reactant utilization, as delineated in Equations (2) and (3) below [10]:

$$P_{H_2} = (1 - U_{f_{H_2}}) \times x\% P_{fuel} \quad (2)$$

$$P_{O_2} = (1 - U_{f_{O_2}}) \times y\% P_{fuel} \quad (3)$$

where $U_{f_{H_2}}$ and $U_{f_{O_2}}$ denote the utilization rates for hydrogen and oxygen, respectively. Additionally, $P_{fuel}$ and $P_{air}$ correspond to the supply pressures, while $x$ and $y$ signify the percentage compositions of the hydrogen and oxygen components.

These reactant utilization rates are mathematically formulated in Equations (4) and (5) as follows [10]:

$$U_{f_{H_2}} = \frac{60000 \times R \times T \times i_{f_c}}{2 \times F \times P_{hydr} \times V_{hydr} \times x\%} \quad (4)$$

$$U_{f_{O_2}} = \frac{60000 \times R \times T \times i_{f_c}}{4 \times F \times P_{oxyg} \times V_{oxyg} \times x\%} \quad (5)$$

where $V_{hydr}$ and $V_{oxyg}$ denote the flow rates for hydrogen and oxygen, respectively, while $i_{f_c}$ represents the fuel cell current.

An oxygen deficit within the cell causes the utilization rate to exceed its nominal value; to account for this deviation, Equation (1) is revised as Equation (6) [10]:

$$E_n = 1.229 + (T - 298) \times \frac{-44.43}{2 \times F} + \frac{R \times T}{2 \times F} \times \ln\left(P_{H_2} \times P_{O_2}^{\frac{1}{2}}\right) - K_u \times \left(U_{f_{O_2}} - U_{f_{O_{2nom}}}\right) \quad (6)$$

where $K_u$ is defined as the voltage drop constant, and $U_{f_{O_{2nom}}}$ represents the nominal oxygen utilization. Furthermore, the open-circuit voltage of a single cell is presented in Equation (7).

$$E_0 = K_C \times E_n \quad (7)$$

where $K_C$ denotes the constant voltage.

By accounting for all cumulative losses including activation, resistive, and diffusion components the voltage of a single cell is expressed as in Equation (8):

$$V = E_0 - V_{act} - V_r \tag{8}$$

where

$$V_{act} = A \times \ln\left(\frac{i_{fc}}{i_0}\right) \times \frac{1}{S \times \frac{T_d}{3}} \tag{9}$$

$$V_r = r_{ohm} \times i_{fc} \tag{10}$$

where $T_d$ represents the cell settling time in response to a current step, and $r_{ohm}$ denotes the cell resistance.

$$A = \frac{R \times T}{2 \times \alpha \times F} \tag{11}$$

and $i_0$ is expressed as follows:

$$i_0 = \frac{2 \times F \times k \times \left(P_{H_2} + P_{O_2}\right)}{R \times h} \times e^{\left(\frac{\Delta G}{R \times T}\right)} \tag{12}$$

where $\alpha$ denotes the charge transfer coefficient, $\Delta G$ represents the activation energy barrier, $k$ is the Boltzmann constant, and $h$ stands for the Planck constant. Consequently, the total voltage of the PEMFC stack is defined as in Equation (13).

$$V_{fc} = N \times V \tag{13}$$

where $N$ represents the number of cells constituting the PEMFC stack.

Utilizing the parameters detailed in Table 1 in conjunction with the mathematical framework established in Equations (1) through (13), the theoretically derived polarization curve for the PEMFC is illustrated in Figure 2.

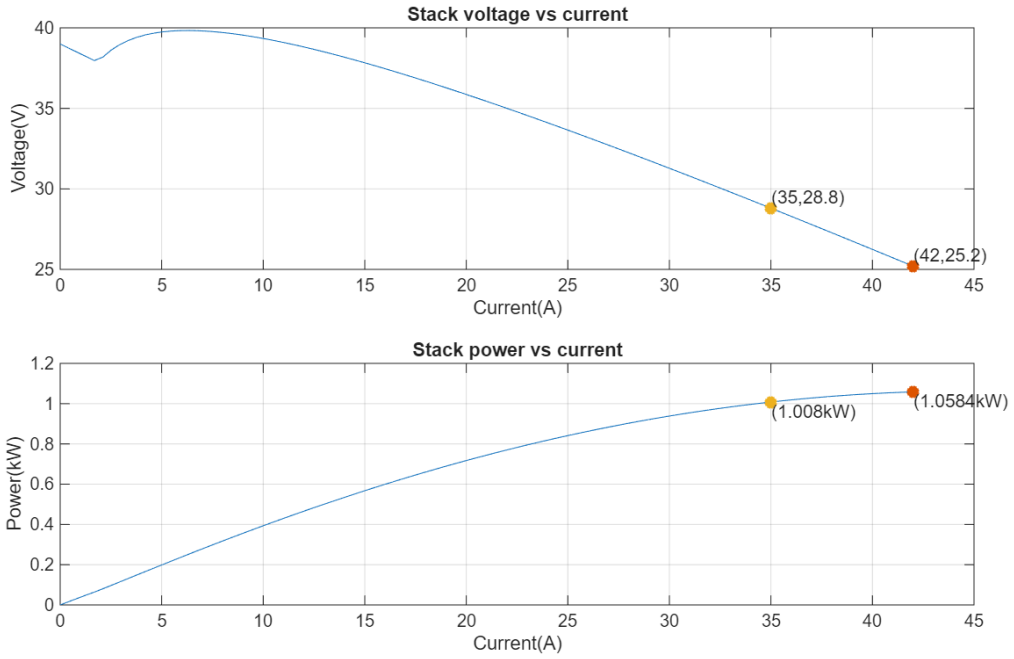


**Figure 2.** Output power and voltage performance characteristics of the 1 kW fuel cell stack.

**Table 1.** Model parameters of the Proton Exchange Membrane Fuel Cell (PEMFC).

| Model Input Parameters For The 1 kW PEMFC Stack | |
|---|---|
| Voltage at 0 A and 1A | 39 V and 36 V |
| Nominal operating point | 35 A and 28.8 V |
| Maximum operating point | 42 A and 25.2 V |
| Number of cells | 48 |
| Nominal stack efficiency | 40% |
| Operating temperature | 30 °C |
| Nominal air flow rate | 130 L per minute |
| Nominal supply pressure | 1.5 bar for hydrogen and 1 bar for oxygen |
| Nominal composition | 100% for hydrogen, 21% for oxygen and 1% for water |

### *2.2. DC-DC Converter*

In this study, a Boost Converter operating at a switching frequency of 10 kHz has been designed, as illustrated in Figure 3, to step up the variable output voltage of the 1 kW PEMFC stack ranging from 25 V to 48 V to 96 V DC bus voltage.

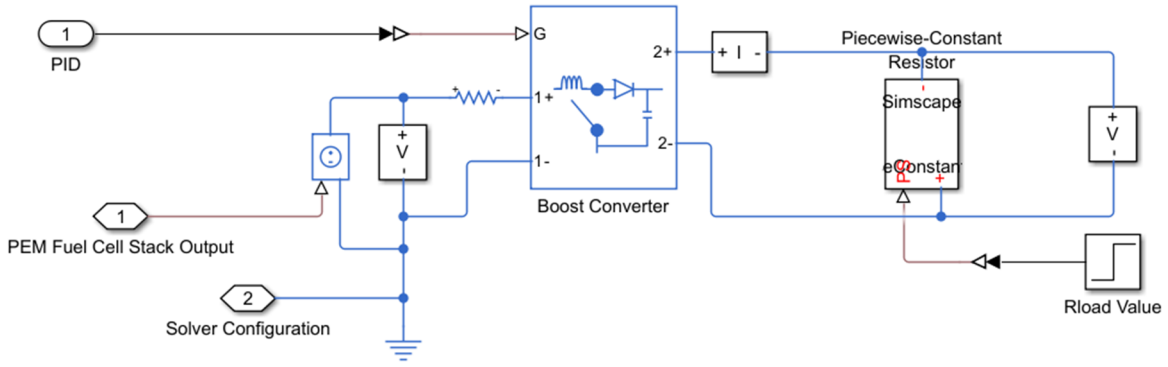


**Figure 3.** Structure of the boost converter.

The data in Figure 2 shows the power output and the voltage of the fuel cell begin at 1.058 kW at around 25.2 volts (V) and 42 amps (A). The converter designed to regulate this unregulated voltage to the output voltage uses an adjustable (duty cycle) process to create the desired output voltage. An inductor and capacitor used as passive elements are used to create a minimal output voltage ripple and allow continuous conduction mode (CCM) of operation at values greater than critical inductance ($L_C$). The calculations for decision making of Critical Inductance is found in the accompanying Equations (14) and (15). The power stage switches at 10 kHz, but the control loop is sampled at a frequency of 200 kHz. Sampling at a higher frequency than the power stage allows a faster, more accurately responsive system to rapid dynamic load variations.

$$L_C = \frac{(1 - D)^2 \times D \times R}{2 \times f} \tag{14}$$

where

$$D = \frac{V_0 - V_{FC}}{V_0} \tag{15}$$

where $f$ denotes the switching frequency and $R$ represents the load.

Inherently discontinuous currents are supplied to the RC network, so the boost converter architecture must include a capacitor filter to attenuate the large voltage ripples produced by high-frequency signals. In the boost converter circuit as shown in Figure 1, the capacitor acts as an energy source for continuous output current. The minimum capacitor value is denoted as $C_{min}$, and the value is calculated as presented in Equation (16).

$$C_{min} = \frac{V_0 - D}{\Delta V_0 \times f \times R} \tag{16}$$

where $\Delta V_0$ represents the output voltage ripple.

The DC-DC boost converter is strictly designed to operate in Continuous Conduction Mode (CCM) to prevent discontinuous input currents that could severely degrade the fuel cell's membrane lifespan. The inductor (L) and capacitor (C) values were specifically calculated to maintain an input current ripple of less than 5% and an output voltage ripple of strictly under 1% at the 10 kHz switching frequency. Furthermore, to accurately reflect the targeted 93% efficiency and realistic thermal losses in the MATLAB/Simulink environment, non-ideal switch models were utilized. Specifically, the internal on-state resistance ($R_{on}$) of the MOSFET and the forward voltage drop ($V_f$) of the power diode were explicitly included in the Simscape component parameters, ensuring the simulation results closely match real-world hardware behavior rather than ideal theoretical assumptions.

The boost converter parameters derived utilizing Equations (14) through (16), are detailed in Table 2.

**Table 2.** Converter parameters.

| Boost Converter Design Parameters | |
|---|---|
| Inductor | $2 \times 10^{-5}$ H |
| Capacitor | $3 \times 10^{-3}$ F |
| Switching frequency | 10 kHz |
| Input voltage | $25 - 48$ V |
| Output voltage | 96 V |
| Efficiency | 93% |
| Load (R) | 10 Ω → 15 Ω (Step Change) |

## 3. Design of the Interval Type-2 Fuzzy Logic System

The proposed controller is architected as an Interval Type-2 Fuzzy Logic System (IT2-FLS), utilizing a Mamdani-type inference engine to effectively address the inherent nonlinearities of the PEMFC powertrain. Fuzzy Logic Systems generally rely on two main inference techniques: the Mamdani method and the Takagi–Sugeno–Kang method. In this study, the Mamdani inference technique is preferred due to its intuitive rule-base representation and its capability to model complex nonlinear systems. The final crisp output of the fuzzy system is obtained through the Center of Gravity (CoG) defuzzification method, as formulated in Equation (17)

$$y^{crisp} = \frac{\sum_{i=1}^{R} q_i \times \int u^{Q^i}}{\sum_{i=1}^{R} \int u^{Q^i}} \tag{17}$$

The controller employs two input variables: Error (e) and Change in Error (ce). Each input variable is represented by five normalized triangular membership functions distributed across the range [−1, 1] (Figure 4). The linguistic terms associated with these inputs are defined as Negative Big (NB), Negative Small (NS), Zero (Z), Positive Small (PS), and Positive Big (PB).

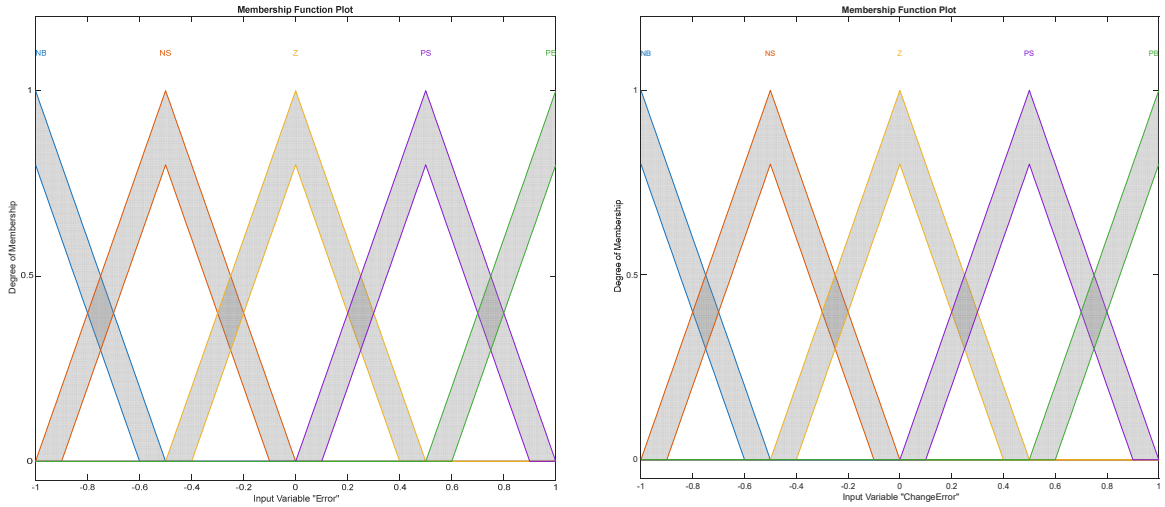


(**a**) Error Membership Function (**b**) ChangeError Membership Function

**Figure 4.** Interval type-2 Input Membership functions for error and changeerror with Footprint of Uncertainty (FOU).

The output variable corresponds to the change in duty cycle (DutyChange) and follows the same linguistic structure (Figure 5).

The control rules have been formulated based on the specified inputs, and the resulting mapping between the input variables and the output is presented in Table 3.

**Table 3.** Fuzzy logic rules.

| $\frac{\Delta E}{E}$ | | Error | | | | |
|---|---|---|---|---|---|---|
| | | **NB** | **NS** | **Z** | **PS** | **PB** |
| Change Error | NB | NB | NB | NB | NS | Z |
| | NS | NB | NB | NS | Z | PS |
| | Z | NB | NS | Z | PS | PB |
| | PS | NS | Z | PS | PB | PB |
| | PB | Z | PS | PB | PB | PB |

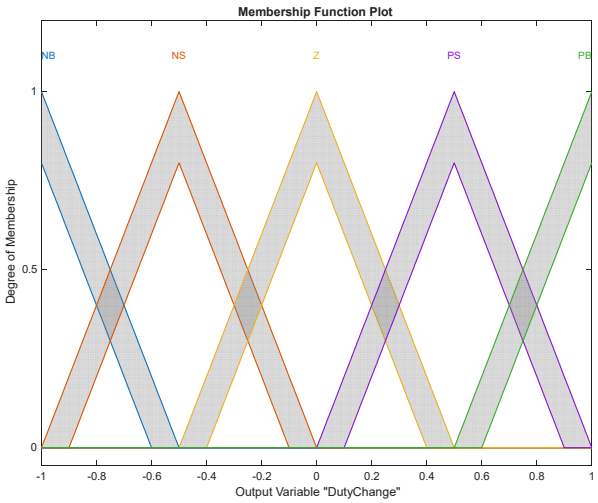


**Figure 5.** Interval Type-2 output membership functions (DutyChange) with Footprint of Uncertainty (FOU).

Unlike conventional Type-1 fuzzy systems, the proposed controller incorporates an Interval Type-2 structure, introducing a Footprint of Uncertainty (FOU) to effectively manage parameter variations and measurement noise. Each membership function is therefore bounded by an Upper Membership Function (UMF) and a Lower Membership Function (LMF). To convert the interval Type-2 fuzzy outputs into crisp control signals, the widely adopted Karnik–Mendel (KM) algorithm is employed for type reduction. The KM algorithm iteratively computes the left and right endpoints of the type-reduced set and yields a bounded type-reduced set, making it computationally suitable for real-time control applications. The final crisp output is obtained as the average of these endpoints.

To ensure full methodological transparency and reproducibility, the key design parameters and normalization settings of the proposed Interval Type-2 Fuzzy Logic Controller (IT2FLC) are summarized in Table 4. This integrated structure confirms that the proposed controller is not a simplified Type-1 extension, but a fully implemented IT2FLC with explicit uncertainty modeling.

**Table 4.** Technical specifications of the designed GS-IT2-FLC.

| Parameter | Value/Selection |
|---|---|
| FIS Type | Mamdani Interval Type-2 |
| Membership Function Shape | Triangular (Interval Type-2) |
| Input Scaling Factors | $G_E = 70$, $G_{CE} = 184$ |
| Output Scaling Factor | $G_U = 20$ |
| Type-Reduction Method | Karnik–Mendel (KM) |
| FOU Lower Scale/Lag | 0.8/[0.2, 0.2] |
| FOU Equivalent Width $(\Delta_\sigma)$ | 0.15 |
| Number of Rules | 25 |
| Rule Weights | 1.0 (Fixed) |

*Proposed Hysteresis Adaptive Gain Scheduling (AGS) Strategy and Threshold Sensitivity*

The core novelty of the proposed scheduling mechanism lies in its departure from conventional single-threshold switching strategies. In traditional approaches, switching between controller gains at a crisp error boundary may introduce undesirable high-frequency chattering. To overcome this, the proposed architecture introduces a dual-threshold hysteresis switching mechanism (Figure 6). By defining separate "Switch-On" and "Switch-Off" thresholds, the logic establishes an overlapping operational band that significantly mitigates chattering during gain transitions.

The operational logic controlling the adaptive gain selection, developed based on the sampling state, is represented mathematically in Equation (18):

$$K(e) = \begin{cases} 4.00, & |e| \geq 2.2 \vee (K_{prev} = 4{,}00 \wedge |e| \geq 1.8) \ (Aggressive) \\ 2.50, & |e| \geq 0.45 \vee (K_{prev} = 2.50 \wedge |e| \geq 0.25) \ (Transition) \\ 1.27, & Otherwise \quad (Fine\ Tuning) \end{cases} \tag{18}$$

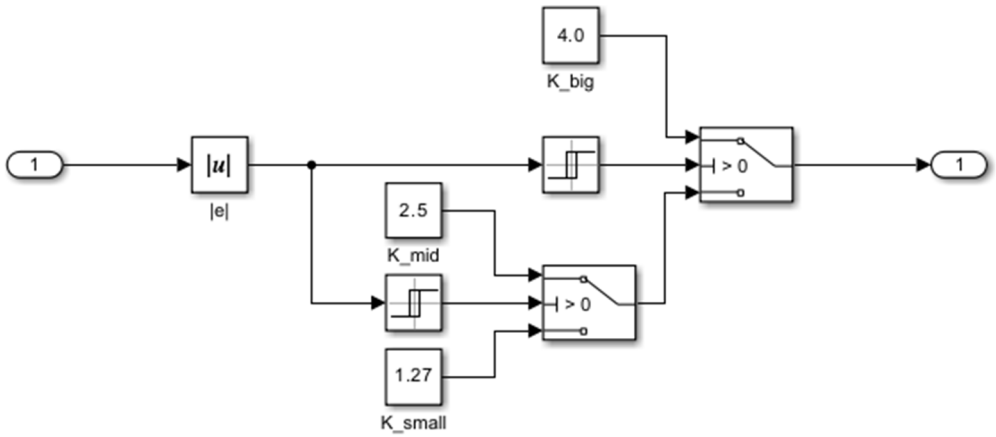


**Figure 6.** Structure of the gain scheduling architecture.

As shown in Equation (18), the system initiates a rapid response during periods of large error, yet maintains its current gain until the error drops below the lower threshold values (1.8 V and 0.25 V). This mechanism enables the controller to react aggressively to abrupt load changes while simultaneously regulating oscillations around the target voltage.

The gain parameters ($K_{big}$ = 4.00, $K_{mid}$ = 2.50, $K_{small}$ = 1.27) and the switching thresholds defined in Equation (18) (2.2 V, 1.8 V, 0.45 V, and 0.25 V) were determined through a systematic iterative tuning procedure based on step-response analysis in the MATLAB/Simulink environment. This design ensures a smooth transition between operating regions while preventing control signal discontinuities. The upper threshold value (2.2 V) was selected to capture major load disturbance conditions, whereas the lower threshold (0.45 V) was intentionally positioned slightly above the steady-state ripple margin to avoid unnecessary controller switching during steady-state operation.

A sensitivity analysis was conducted to evaluate the influence of threshold variations on system performance. The results indicate that narrowing the hysteresis band increases the system's sensitivity to voltage noise and may reintroduce control signal chattering. Conversely, excessively widening the hysteresis band delays the transition to the fine-regulation region, resulting in increased settling time and larger transient overshoot. Furthermore, the efficient switching logic ensures low computational overhead, which makes the proposed controller suitable for real-time embedded implementation in electronic control units (ECUs).

## 4. Simulation Results and Discussion

The performance of the parameter-optimized Gain-Scheduled Interval Type-2 Fuzzy Logic Controller (GS-IT2-FLC) was compared with the industrial-standard Proportional-Integral (PI) controller using a 1 kW Proton Exchange Membrane Fuel Cell (PEMFC) power system model operating at a 10 kHz switching frequency. To ensure scientific rigor and a fair comparison, both controllers were evaluated under identical system conditions, including the same converter configuration, duty-cycle limits of [0.35, 0.87], and identical simulation initialization parameters.

The baseline PI controller was implemented as a discrete-time controller with a proportional gain $K_p$ = 0.02, an integral gain $K_i$ = 7, and a sampling time of 0.0001 s, corresponding to the switching period of the converter. To prevent integrator saturation during large transient errors occurring at startup, a back-calculation anti-windup mechanism with a gain of 1 was incorporated into the controller structure. For consistency in the cold-start scenario, the fuzzy controller branch was initialized with a discrete-time integrator initial condition of 0.7, ensuring a comparable starting point for the control signal generation.

### *4.1. Simulation Framework and Test Sequence*

To ensure the reproducibility of the results, the following test sequence was implemented in the MATLAB/Simulink environment:

- Initial State: The system starts from a zero-voltage state ($V_{out}$ = 0 V) to analyze the cold-start behavior.
- Load Step Timing: The load resistance is initially set to 10 Ω and is stepped up to 15 Ω at $t$ = 0.15 s to evaluate the dynamic response.
- Solver Settings: The simulation utilizes a fixed-step solver (ode4) with a sample time of $5 \times 10^{-6}$ s (200 kHz) to match the control loop frequency.

- Disturbances: No additional artificial noise was added to isolate and observe the controller's inherent response to the non-linear polarization of the fuel cell.

The main controller and simulation parameters are summarized in Table 5.

**Table 5.** Controller and simulation framework parameters.

| Parameter | Value |
|---|---|
| Switching Frequency | 10 kHz |
| Control Sampling Time | 0.0001 s (100 µs) |
| PI Proportional Gain ($K_p$) | 0.02 |
| PI Integral Gain ($K_i$) | 7 |
| PI Anti-windup Gain | 1 |
| Duty Cycle Limits | [0.35, 0.87] |
| Fuzzy Integrator Initial Condition | 0.7 |
| Load Step Sequence | 10 Ω to 15 Ω at $t$ = 0.15 s |
| Simulation Solver | Fixed-step (ode4) |

### *4.2. Dynamic Response Characteristics and Cold-Start Analysis*

The cold-start phase is one of the most critical periods determining the operational reliability of power systems. From a stability perspective, the cold-start condition represents the most demanding operating scenario, as the slow electrochemical dynamics of the fuel cell must align with the instantaneous electrical response of the DC-DC converter.

#### 4.2.1. Behavior of the Traditional PI Controller

The technical examination of the simulation results revealed significant transient oscillations in the response of the PI controller. Due to its fixed-gain architecture, the controller is susceptible to integral wind-up, resulting in control signal saturation and risking hardware overload. As shown in Figure 7, the system exhibited a risky overshoot, exceeding the reference value by 76.45% at start-up. Consequently, as illustrated in Figure 8, this uncontrolled voltage spike triggered a sudden current impulse reaching 16.94 A on the source side, forcing components to their thermal and mechanical limits.

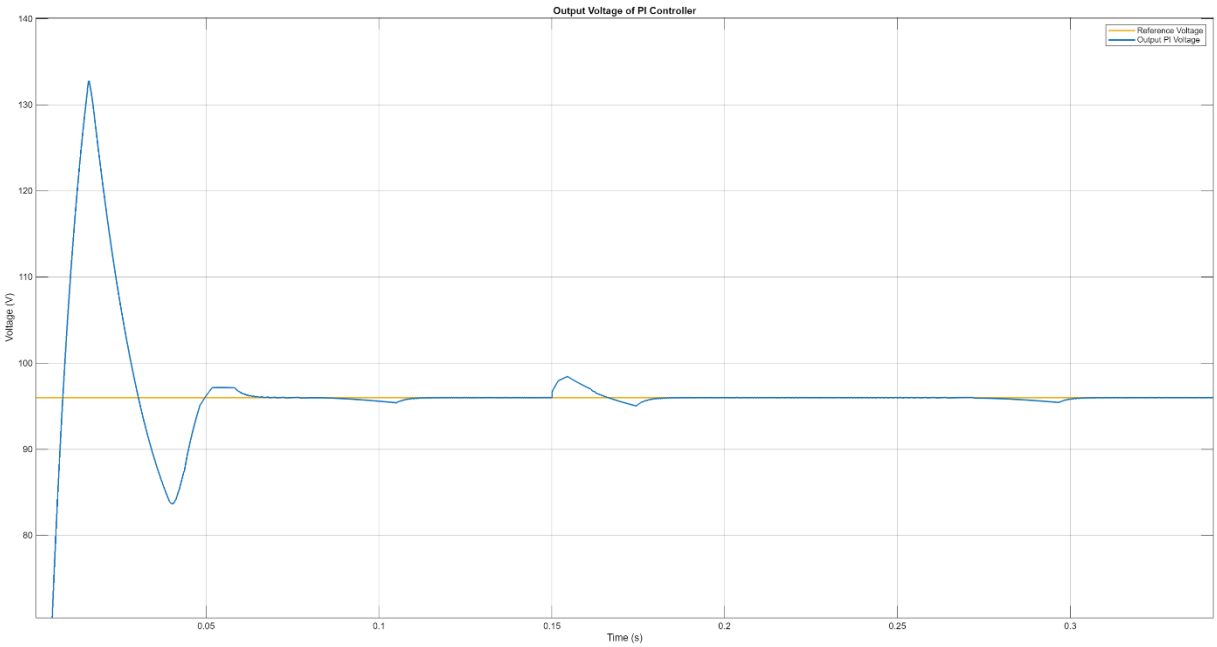


**Figure 7.** Output voltage response of the traditional Proportional-Integral controller (the red circle and zoomed-in window demonstrate the high overshoot problem of 76.45% at start-up and system instability).

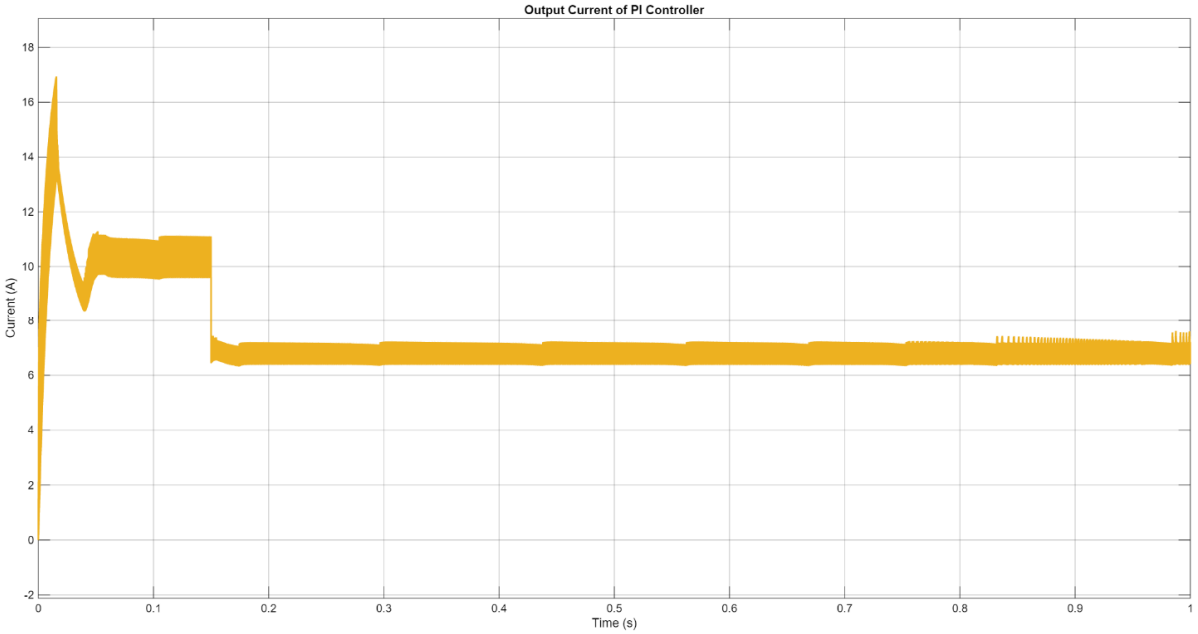


**Figure 8.** Proton exchange membrane fuel cell stack current and resulting inrush current under Proportional-Integral controller (Peak value: 16.94 A).

### 4.2.2. Behavior of the Proposed GS-IT2-FLC

In the proposed GS-IT2-FLC architecture, the Footprint of Uncertainty (FOU) and the hysteresis adaptive gain scheduling mechanism significantly improved overall behavior. This mechanism rapidly damped the start-up deviation by dynamically optimizing gains as the error increased. As illustrated in Figure 9, the voltage overshoot was pulled down to 24.12%, and the system settled into a stable state in just 0.30 s, establishing superiority in dynamic performance. Furthermore, as demonstrated in Figure 10, the proposed controller effectively limited the peak stack current to 11.92 A, preventing severe inrush currents and validating its enhanced hardware protection capabilities.

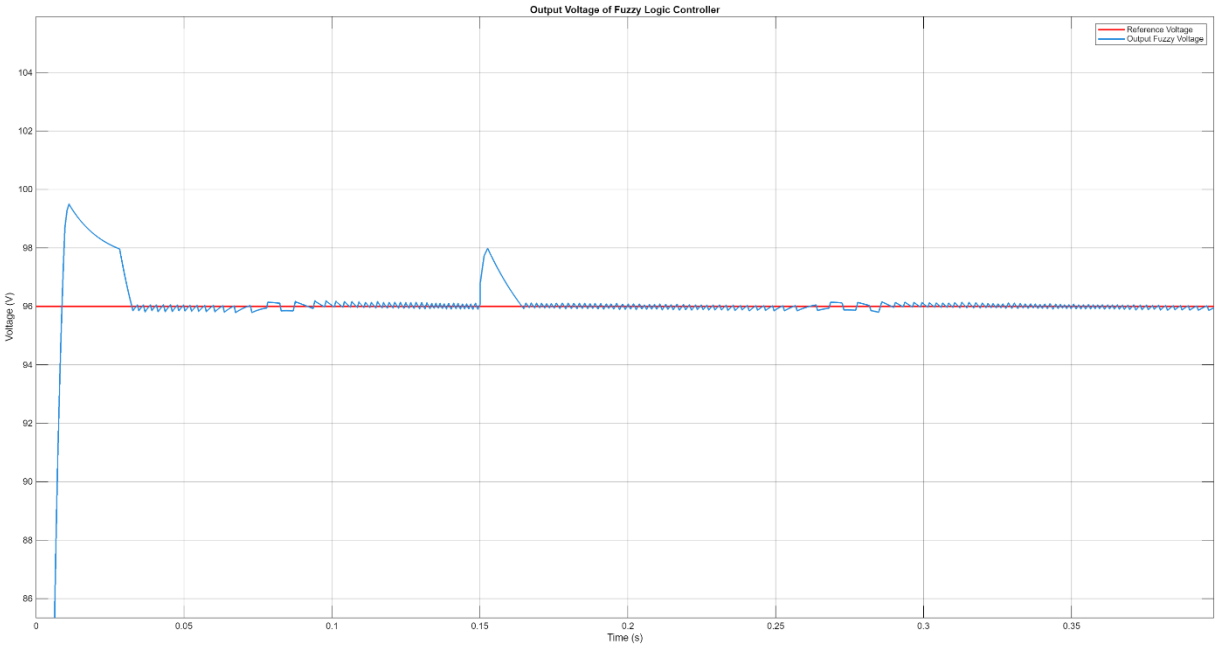


**Figure 9.** Output voltage response of the proposed Gain-Scheduled Interval Type-2 Fuzzy Logic structure (the zoomed-in window proves that the overshoot is suppressed to 24.12% and the system stabilizes rapidly).

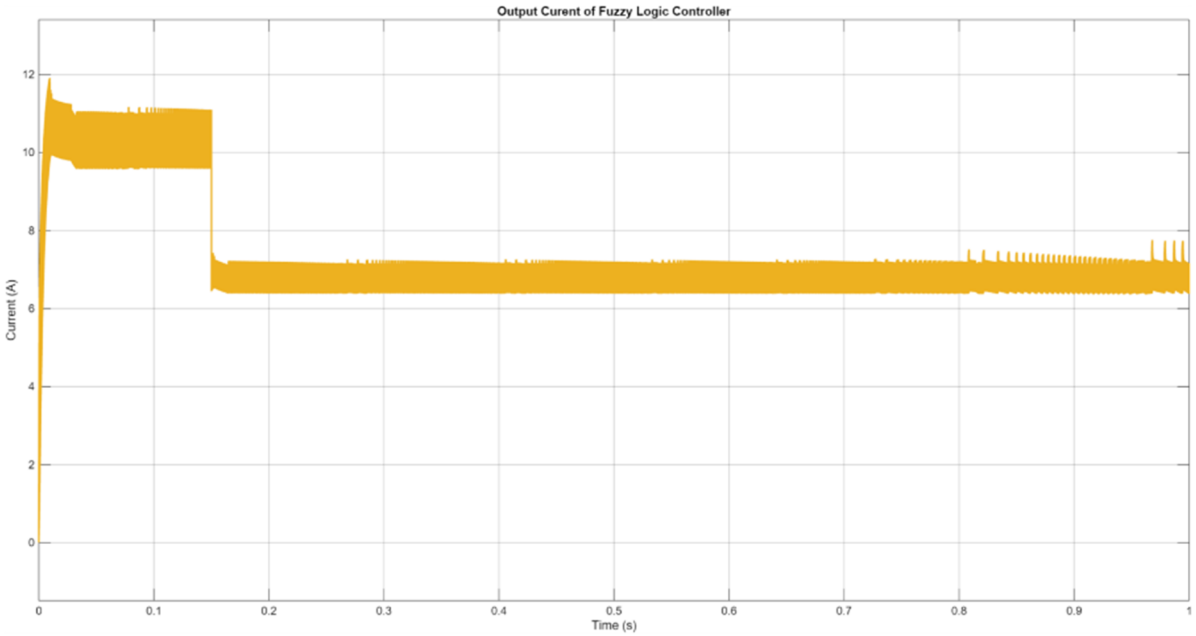


**Figure 10.** Stack current limited by the Gain-Scheduled Interval Type-2 Fuzzy Logic Controller (11.92 A) and hardware protection performance.

### *4.3. Power Analysis and Thermal Stress Evaluation*

Power analysis revealed that the aggressive transient response of the PI controller resulted in a peak power of 2869.3 W, introducing considerable electrothermal stress on the power electronic components and the fuel cell stack. Conversely, as corroborated by the hardware protection performance in Figure 11 and the output power response in Figure 12, the GS-IT2-FLC limited this peak power to 1419.8 W through adaptive and soft duty cycle changes, maintaining hardware safety.

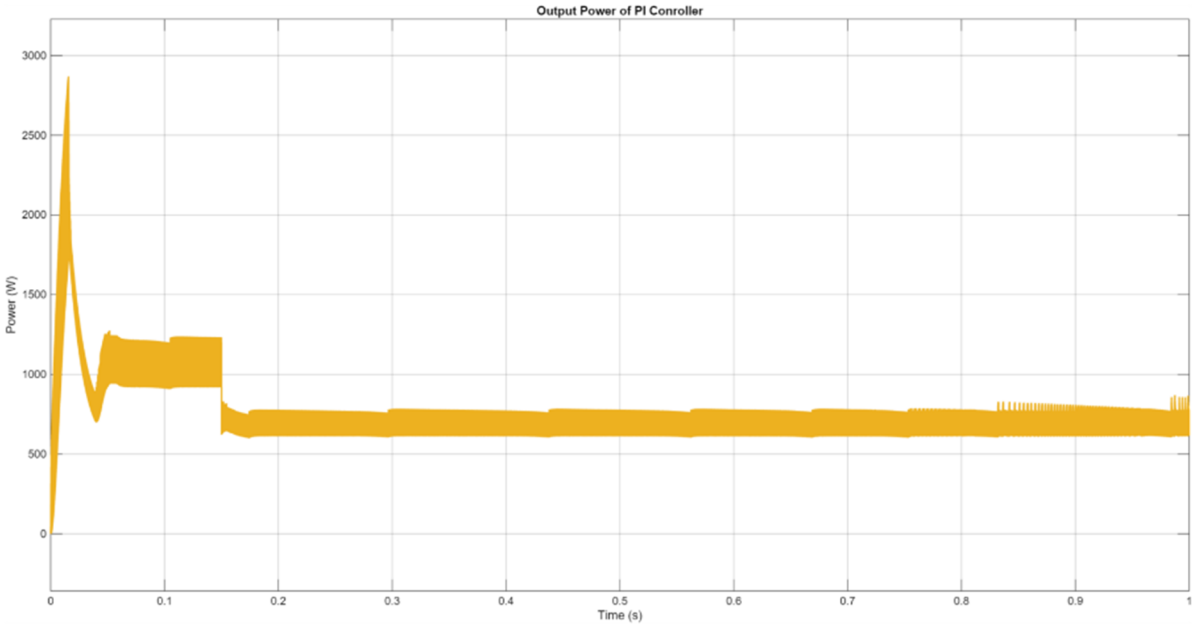


**Figure 11.** Stack current limited by the Gain-Scheduled Interval Type-2 Fuzzy Logic Controller (11.92 A) and hardware protection performance.

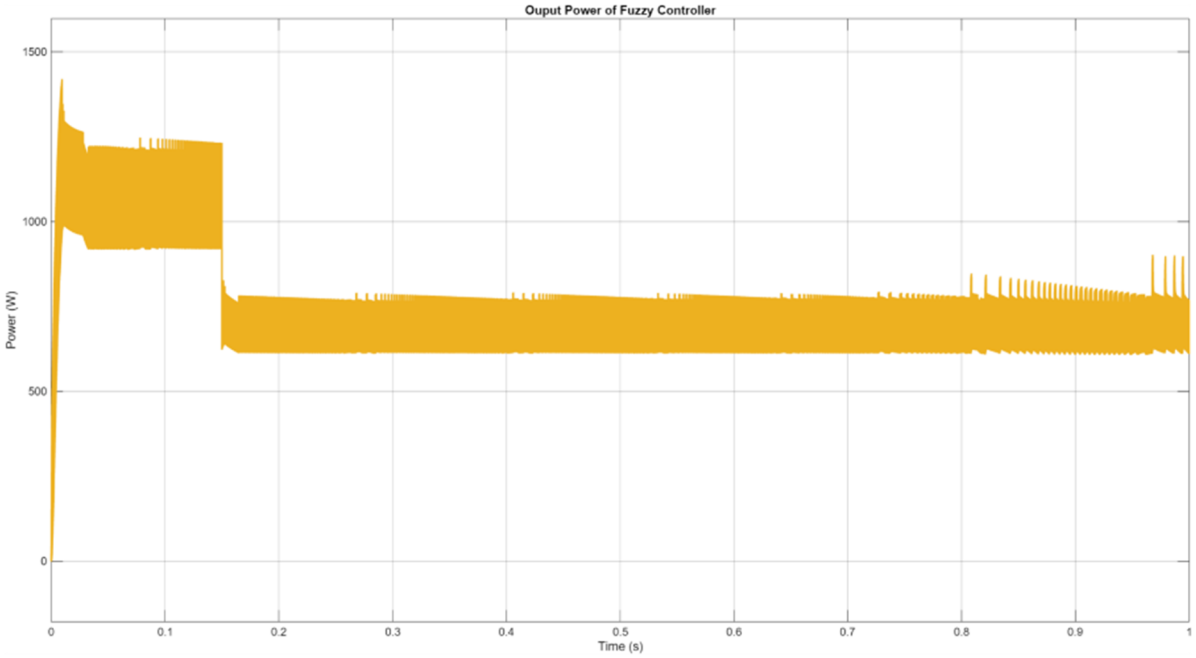


**Figure 12.** Output power response determining the thermal stress on power components for both controllers (soft start-up and stress management with GS-IT2-FLC).

### *4.4. Numerical Performance and Engineering Implications*

The comparative performance indicators presented in Table 6 clearly demonstrate the superiority of the proposed controller in terms of transient regime safety and hardware preservation, while maintaining steady-state accuracy.

**Table 6.** Comparative performance metrics of PI and GS-IT2-FLC controllers.

| Performance Indicator | Proportional-Integral Controller | Gain-Scheduled Interval Type-2 Fuzzy Logic | Engineering Interpretation/Design Implication |
|---|---|---|---|
| Average Output Voltage ($t \geq 0.3$ s) | 95.94 V | 96.04 V | Both structures offer similar steady-state accuracy; the proposed structure provides regulation closer to the reference. |
| Voltage Overshoot | 76.45% | 24.12% | Reducing the startup overshoot by approximately two-thirds (68.4%) provides a critical safety advantage for the fuel cell and power switches. |
| Transient Response Behavior | Significant transient oscillations | Rapid damping (<0.3 s) | The rapidly damped transient regime ensures the system behaves more predictably under sudden load and start-up conditions. |
| Peak Stack Current | 16.94 A | 11.92 A | The 29.6% reduction in current peak translates to lower electrothermal stress on semiconductor elements and the fuel cell stack. |
| Peak Output Power | 2869.3 W | 1419.8 W | 50.5% reduction contributing to improved system reliability and reduced thermal stress. |

The substantial reductions in voltage overshoot (68.4%), peak current (29.6%), and peak power (50.5%) are critically important for preserving the electrochemical integrity of the fuel cell stack and ensuring power electronic components operate within safe thermal limits. By mitigating instantaneous peak power stress, recognized as a key contributor to accelerated membrane degradation, the proposed controller delivers practical hardware-aware benefits that enhance the long-term operational reliability of PEMFC systems. These results confirm that the proposed control strategy effectively balances dynamic performance and hardware protection, which is a key requirement in practical PEMFC applications.

## 5. Conclusions

The hybrid Gain-Scheduled Interval Type-2 Fuzzy Logic Controller (GS-IT2-FLC) architecture proposed in this study was developed to address the dual requirement of maintaining stable voltage regulation in Proton Exchange Membrane Fuel Cell (PEMFC) power systems while simultaneously reducing electrical stress on power electronic components. The simulation-based validation of the proposed architecture demonstrates several important contributions to advanced control strategies for renewable energy systems.

The adaptive gain-scheduling mechanism significantly improves transient safety during the cold-start phase, which represents one of the most critical operating conditions of PEMFC systems. The voltage overshoot was reduced from 76.45% to 24.12%, providing a substantial improvement in operational safety for both the fuel cell stack and the associated power electronic components.

The proposed GS-IT2-FLC also achieves steady-state voltage regulation accuracy comparable to that of a conventional PI controller (approximately 96.04 V), while providing a more robust dynamic response by suppressing high-amplitude transient oscillations and enabling the system to reach a stable operating condition in less than 0.30 s.

Furthermore, the proposed control architecture significantly mitigates hardware stress by reducing the instantaneous peak power from 2869.3 W to 1419.8 W, corresponding to a reduction of approximately 50.5%. Limiting such transient peaks plays an important role in reducing electrothermal stress, which is widely recognized as a major factor contributing to the degradation of fuel cell membranes and power electronic components.

Overall, the results indicate that selecting an appropriate control strategy represents a critical engineering trade-off between computational simplicity and system protection. While classical PI controllers remain suitable for applications with strict computational constraints, they inherently expose the powertrain to higher transient stress. In contrast, the proposed GS-IT2-FLC architecture provides a more balanced and safety-oriented control solution for PEMFC power systems where hardware protection, operational stability, and long-term system reliability are primary design priorities.

### Author Contributions

M.F.: conceptualization, methodology, software (power electronics and converter design), investigation, visualization, writing—original draft preparation (Sections 3–5), writing—review and editing; D.M.K.: conceptualization, methodology, software (control architectures), investigation, visualization, writing—original draft preparation (Abstract, Introduction, Sections 2–4), writing—review and editing; G.B.: supervision, validation, writing—review and editing. All authors have read and agreed to the published version of the manuscript.

### Institutional Review Board Statement

Not applicable.

### Informed Consent Statement

Not applicable.

### Data Availability Statement

The data presented in this study are available on request from the corresponding author.

### Conflicts of Interest

The authors declare no conflict of interest.

### Use of AI and AI-Assisted Technologies

During the preparation of this work, the author(s) used Google NotebookLM to assist with the literature review and ensure a comprehensive analysis of the referenced articles, and Google Gemini to edit grammar and improve the language of the manuscript. After using these tools/services, the author(s) reviewed and edited the content as needed and take(s) full responsibility for the content of the published article.

## References


1. El Aimani, S. Modeling and simulation of a hydrogen-based proton exchange membrane fuel cell for power generation. In Proceedings of the 2023 5th Global Power, Energy and Communication Conference (GPECOM), Nevsehir, Turkey, 14–16 June 2023; pp. 381–387.
2. Fandi, G.; Novák, J.; Chyský, J.; et al. Review and modeling on hydrogen fuel cells electric vehicle (HFCEV), in comparison with battery electrical vehicle (BEV) using MATLAB environment. Case study: Postal car. *Energy Convers. Manag. X* **2024**, *24*, 100684.
3. Ko, J.S.; Huh, J.H.; Kim, J.C. Overview of maximum power point tracking methods for PV system in micro grid. *Electronics* **2020**, *9*, 816.
4. Harrag, A.; Messalti, S. How fuzzy logic can improve PEM fuel cell MPPT performances? *Int. J. Hydrog. Energy* **2018**, *43*, 537–550.
5. Harrag, A.; Messalti, S. IC-based variable step size neuro-fuzzy MPPT improving PV system performances. *Energy Procedia* **2019**, *157*, 362–374.
6. Doğan, S.; Haydaroğlu, C.; Gümüş, B.; et al. Innovative fuzzy logic type 3 controller for transient and maximum power point tracking in hydrogen fuel cells. *Int. J. Hydrog. Energy* **2025**, *143*, 833–845.
7. Rezk, H.; Fathy, A. Performance improvement of PEM fuel cell using variable step-size incremental resistance MPPT technique. *Sustainability* **2020**, *12*, 5601.
8. Derbeli, M.; Barambones, O.; Silaa, M.Y.; et al. Real-time implementation of a new MPPT control method for a DC-DC boost converter used in a PEM fuel cell power system. *Actuators* **2020**, *9*, 105.
9. Kim, J.C.; Huh, J.H.; Ko, J.S. Optimization design and test bed of fuzzy control rule base for PV system MPPT in micro grid. *Sustainability* **2020**, *12*, 3763.
10. Luta, D.N.; Raji, A.K. Fuzzy rule-based and particle swarm optimisation MPPT techniques for a fuel cell stack. *Energies* **2019**, *12*, 936.
11. Charaabi, A.; Barambones, O.; Zaidi, A.; et al. A novel two stage controller for a DC-DC boost converter to harvest maximum energy from the PV power generation. *Actuators* **2020**, *9*, 29.
12. Benchouia, N.E.; Derghal, A.; Mahmah, B.; et al. An adaptive fuzzy logic controller (AFLC) for PEMFC fuel cell. *Int. J. Hydrog. Energy* **2015**, *40*, 13806–13819.
13. Abbaspour, A.; Khalilnejad, A.; Chen, Z. Robust adaptive neural network control for PEM fuel cell. *Int. J. Hydrog. Energy* **2016**, *41*, 20385–20395.
14. Gwon, M.G.; Lee, K.C.; Kim, J.M. Development of DC–DC converters for fuel-cell hybrid power systems in a lift–cruise unmanned aerial vehicle. *Energies* **2025**, *18*, 5688.
15. Du, J.; Zhang, X.; Wang, S.; et al. A novel ANFIS-dynamic programming fusion strategy for real-time energy management optimization in fuel cell electric commercial vehicles. *Electronics* **2025**, *14*, 4601.
16. Mazouzi, A.; Hadroug, N.; Alayed, W.; et al. Comprehensive optimization of fuzzy logic-based energy management system for fuel-cell hybrid electric vehicle using genetic algorithm. *Int. J. Hydrog. Energy* **2024**, *81*, 889–905.
17. Luo, X.; Chung, H.S.H. EMS for hydrogen fuel cell electric vehicles based on improved fuzzy control. *Energy Convers. Manag. X* **2025**, *27*, 101093.
18. Yuan, S.; Hua, Q.; Shuai, Q.; et al. Energy management and performance improvement for fuel cell hybrid electric vehicle with reinforcement learning-based dual model predictive control. *Int. J. Hydrog. Energy* **2025**, *185*, 151770.
19. García, P.; García, C.A.; Fernández, L.M.; et al. ANFIS-based control of a grid-connected hybrid system integrating renewable energies, hydrogen and batteries. *IEEE Trans. Ind. Inform.* **2013**, *10*, 1107–1117.
20. Çakmak, R.; Bayrak, G.; Koç, M. A fuzzy logic-based energy management approach for fuel cell and photovoltaic powered electric vehicle charging station in DC microgrid operations. *IEEE Access* **2025**, *13*, 49905–49921.
21. Bizon, N.; Thounthong, P. Energy efficiency and fuel economy of a fuel cell/renewable energy sources hybrid power system with the load-following control of the fueling regulators. *Mathematics* **2020**, *8*, 151.
22. Bayrak, G.; Basaran, K.; Lazaroiu, A.C. Integrating hydrogen-powered fuel cell electric buses into grid-forming microgrids: A solution for emergency energy needs. *Renew. Energy* **2025**, *250*, 123363.
23. Bayrak, G.; Das, M. Enhancing grid resilience and cybersecurity considering visible light communication in electric vehicle charging units powered by green hydrogen. *Int. J. Hydrog. Energy* **2025**, *144*, 819–837.